Local spin-density-wave order inside vortex cores in multiband superconductors

Vivek Mishra and Alexei E. Koshelev
Materials Science Division, Argonne National Laboratory, Lemont, IL 60439, USA
(Dated: August 13, 2015)

Coexistence of antiferromagnetic order with superconductivity in many families of newly discovered iron-based superconductors has renewed interest to this old problem. Due to competition between the two types of order, one can expect appearance of the antiferromagnetism inside the cores of the vortices generated by the external magnetic field. The structure of a vortex in type II superconductors holds significant importance from the theoretical and the application points of view. Here we consider the internal vortex structure in a two-band $s_\pm$ superconductor near a spin-density-wave instability. We treat the problem in a completely self-consistent manner within the quasiclassical Eilenberger formalism. We study the structure of the $s_\pm$ superconducting order and magnetic field-induced spin-density-wave order near an isolated vortex. We examine the effect of this spin-density-wave state inside the vortex cores on the local density of states.

PACS numbers: 74.20.De, 74.25.Op, 74.25.Ha

I. INTRODUCTION

The emergence of superconductivity at the onset of magnetism is a hallmark of many families of unconventional superconductors. Recently discovered iron based superconductors (FeSCs) provided a new addition to this list. Parent compounds for many of the FeSCs have the spin-density-wave (SDW) order, and superconductivity (SC) appears upon doping or under pressure.[1–6] The doping-temperature phase diagrams describing location of these two phases vary from material to material. In some systems, for example in the 1111 family $RFeAsO_{1-x}F_x$ (R is a rare-earth element), the SDW phase abruptly disappears once the SC phase develops. In other systems, such as 122 compounds based on $BaFe_2As_2$, the SDW order coexists with SC within some range of parameters.

To understand how the SDW and SC phases interact with each other and what triggers superconductivity with such high transition temperatures, knowledge of the precise structure of order parameters is essential. The local electronic structure near defects can be extracted from scanning tunneling spectroscopy (STM) measurements and it provides vital information about the order parameter. A Defect could be either an impurity or a topological singularity like a vortex induced by magnetic field. Here we focus on structure of an isolated vortex.

It is well known that the shape of the vortex and the electronic structure close to it are very sensitive to the gap structure.[7] Copper oxide based high-temperature superconductors have been subjected to extensive research for various kinds of competing orders inside the vortex cores. The signatures of such vortex-core orders have been reported in $Bi_2Sr_2CaCu_2O_{8+\delta}$,[8] $La_{2-\delta}Sr_\delta CuO_4$,[9–15] $YBa_2Cu_3O_{7-\delta}$,[16–21] $YBa_2Cu_4O_8$,[22] and $Tl_2Ba_2CuO_{6+\delta}$.[23] From the standpoint of the theory, several different approaches have been adopted to explain these experimental observations. Arovas *et al.*[24] and Sachdev *et al.*[25] studied antiferromagnetism in the vortex cores within phenomenological Ginzburg-Landau free-energy functional method. Ghosal *et al.*[26] used microscopic Bogoliubov-de Gennes (BdG) technique to investigate this problem for the superconductors with a d-wave symmetric order parameter. The BdG technique was used heavily by many researchers to understand various aspects of the competing orders inside the vortex cores.[27–30] We also mention the work of Garkusha *et al.*[31] where the Usadel equation formalism has been used to explore the problem of antiferromagnetic vortex cores. The Usadel equations, however, are only applicable in the dirty limit, when the electronic mean free path is shorter than the coherence length, hence only appropriate for s-wave superconductors.

The vortex state in FeSCs has been studied extensively by the STM[32] and several novel features near vortex cores have been revealed. In the first study of the vortex structure in the optimally-doped $BaFe_{1.8}Co_{0.2}As_2$ by Yin *et al.*[33] no subgap states have been found. This is most probably due to large quasiparticle scattering rate in this material. On the other hand, optimally-doped $Ba_{0.6}K_{0.4}Fe_2As_2$ does show peak at the vortex center, which is shifted from the Fermi level to lower energy.[34] This shift was attributed to the quantum effect, which is realized in the materials with moderate values of the product of the Fermi momentum k_F and the coherence length ξ_0 at temperatures lower than $T_c/(k_F\xi_0)$. Alternatively, such energy shift of the localized state which breaks the particle-hole symmetry can be caused by magnetic field-induced order in the vortex core. This scenario is very likely when a superconductor is close to a SDW instability. This possibility, however, has not been considered in Ref. 34. Similar downshift was found in LiFeAs by Hanaguri *et al.*,[35] even though this material does not have obvious proximity to magnetism. Song *et al.*[36] studied the vortex state in FeSe and found enhanced C_4 symmetry breaking in the vortex core which is probably related to orbital order in this material.

These compelling features have motivated many theoretical works. One class of theories has associated the particle-hole asymmetric finite-energy peaks to the

normal-state band structure of the materials.[37,38] In this case the mechanism of particle-hole symmetry breaking is due to the quantum effect discussed in Ref. 39. Contrary to this proposal, several other authors have considered orbital[40], nematic[41] or SDW order[42–44]. Hung *et al.*[40] have included orbital ordering within a self-consistent BdG approach, and explained the enhanced C_4 symmetry breaking observed in FeSe by Song *et al.* in Ref. 36. Similar results were reported by Jiang *et al.*[42] and Hu *et al.*[43] for the SDW order also using the BdG method.

In this paper, we consider the emergence of the SDW order in the vortex cores and its spectroscopic consequences. We use the quasiclassical Eilenberger approach to study the problem of the field-induced SDW order inside an isolated vortex. Both the BdG and Eilenberger approaches have their own advantages and complement each other. The BdG method is more microscopic. On the other hand, the Eilenberger approach relies on few most essential physical parameters. It is numerically less expensive and allows to study more complex problems. We compute distribution of the superconducting and SDW order parameters inside the core and typical length scales for both order parameters. We also investigate influence of emerging SDW order on the density of states (DOS) near the vortex. This paper is organized in the following manner. In the next Sec. II, we describe the details of the model and the method. In Sec. III we discuss the results and conclude in Sec. IV.

II. MODEL & METHOD

A. Quasiclassical equations for a two-band superconductor with spin-density wave

We consider a simple minimal model with two cylindrical Fermi surfaces, which allows us to capture qualitative understanding of the problem. For the dispersion of the holelike Fermi surface, we take

$$\xi_h(\mathbf{k}) \equiv \xi_1(\mathbf{k}) = \mu_h - \frac{k^2}{2m_h}, \tag{1}$$

and for the electronlike Fermi surface we consider following dispersion,

$$\xi_e(\mathbf{k}) \equiv \xi_2(\mathbf{k}-\mathbf{Q}) = \frac{(k_x-Q_x)^2}{2m_e(1-\epsilon)} + \frac{(k_y-Q_y)^2}{2m_e(1+\epsilon)} - \mu_e, \tag{2}$$

where (Q_x,Q_y) is the SDW ordering vector and μ_h,μ_e are the energy offset for the hole and the electron band respectively. Fig. 1 shows a schematic picture of the two Fermi surfaces. It is useful to write these dispersions as,

$$\xi_h(\mathbf{k}) = -\xi, \tag{3}$$
$$\xi_e(\mathbf{k}+\mathbf{Q}) = \xi + 2\delta, \tag{4}$$

where δ is the energy scale, which measures the deviation from perfect nesting. In general, δ is a function of the angle on the Fermi surface ϕ and goes to zero at the hot spots (shown in Fig 1). For the dispersions considered here,

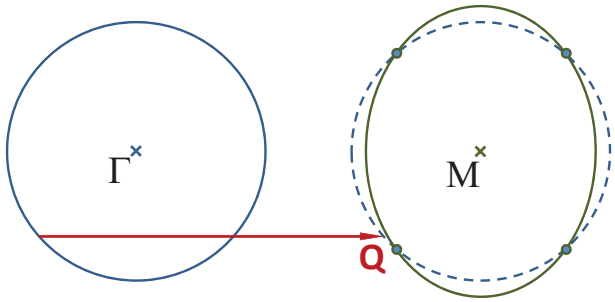

FIG. 1. (Color online) Schematic representation of the holelike and electronlike Fermi surfaces (solid lines) centered around the Γ point and M point respectively. A shifted holelike Fermi surface is shown with dashed line. Filled circles are the hot spots, where the nesting is perfect.

$$\delta(\phi) = \delta_{\rm iso} + \delta_{\rm ani}\cos 2\phi, \tag{5}$$

with

$$\delta_{\rm iso} = \frac{1}{2}\left(\frac{m_h\mu_h}{m_e(1-\epsilon^2)} - \mu_e\right),$$
$$\delta_{\rm ani} = \frac{m_h\mu_h}{2m_e}\frac{\epsilon}{1-\epsilon^2},$$

and we treat $\delta_{\rm iso}$ and $\delta_{\rm ani}$ as tuning parameters.

The model Hamiltonian is same as used by several other groups[45–47],

$$\mathbf{H} = \mathbf{H}_{\rm kin} + \mathbf{H}_{\rm sc} + \mathbf{H}_{\rm sdw}, \tag{6}$$
$$\mathbf{H}_{\rm kin} = \sum_{i,\mathbf{k},\alpha} \xi_i(\mathbf{k}) c^\dagger_{i,\mathbf{k},\alpha} c_{i,\mathbf{k},\alpha}, \tag{7}$$
$$\mathbf{H}_{\rm sc} = \sum_{i,\mathbf{k},\alpha,\beta} \left[\Delta_i \left(\imath\sigma^y\right)_{\alpha\beta} c^\dagger_{i,\mathbf{k},\alpha} c^\dagger_{i,-\mathbf{k},\beta} + h.c.\right], \tag{8}$$
$$\mathbf{H}_{\rm sdw} = \sum_{\mathbf{k},\alpha,\beta} \left[M^* \left(\sigma^z\right)_{\alpha\beta} c^\dagger_{1,\mathbf{k},\alpha} c_{2,\mathbf{k},\beta} + h.c.\right], \tag{9}$$

where Δ_i are the SC order parameters for two bands with $i = 1, 2$ being the band index and M is the SDW order parameter. We only consider singlet superconductivity. For incommensurate SDW order M is a complex quantity. Here we consider only the commensurate SDW order, which makes M a real quantity. We will briefly discuss the consequences of incommensurability in the SDW order. The indices α, β denote the spin states, and $c^\dagger_{i,\mathbf{k},\alpha}$ ($c_{i,\mathbf{k},\alpha}$) is the fermionic creation (annihilation) operator for a fermion in the $i^{\rm th}$ band with spin α. We consider $s_\pm$ state for superconductivity with equal gap magnitudes in two bands with a relative sign change.

The self-consistency conditions read,

$$\Delta_i = \sum_{j,\mathbf{k},\alpha,\beta} V^{\rm sc}_{ij} \left(-\imath\sigma^y\right)_{\alpha\beta} \left\langle c_{j,-\mathbf{k},\alpha} c_{j,\mathbf{k},\beta}\right\rangle, \tag{10}$$
$$M = \sum_{k,\alpha,\beta} V^{\rm sdw} \left(\sigma^z\right)_{\alpha\beta} \left\langle c^\dagger_{1,\mathbf{k},\alpha} c_{2,\mathbf{k},\beta}\right\rangle. \tag{11}$$

Here $V^{\rm sc}$ and $V^{\rm sdw}$ are the pairing interactions for the SC and SDW phases respectively and assumed to be momentum independent.

In the extended particle-hole basis, $\Psi^\dagger = \left(c^\dagger_{1,\mathbf{k},\uparrow}, c_{1,-\mathbf{k},\downarrow}, c^\dagger_{2,\mathbf{k},\uparrow}, c_{2,-\mathbf{k},\downarrow}\right)$, the Hamiltonian reads,

$$\mathbf{H} = \sum_k \Psi^\dagger \cdot \hat{\mathcal{H}} \cdot \Psi, \tag{12}$$

$$\hat{\mathcal{H}} = \begin{bmatrix} \xi_1 & \Delta_1 & M & 0 \\ \Delta_1^* & -\xi_1 & 0 & M \\ M & 0 & \xi_2 & \Delta_2 \\ 0 & M & \Delta_2^* & -\xi_2 \end{bmatrix}. \tag{13}$$

The 4×4 matrix Green's function for this mean-field Hamiltonian is

$$\hat{\mathcal{G}} = \left(i\omega\hat{\mathbb{1}} - \hat{\mathcal{H}}\right)^{-1}, \tag{14}$$

where $\omega = 2\pi T(n+1/2)$ is the fermionic Matsubara frequency and $\hat{\mathbb{1}}$ is 4×4 identity matrix in the two band particle-hole space.

Next, we derive the quasiclassical equations, which were first obtained by Eilenberger for conventional superconductors[48,49]. These are transportlike equations for the kinetic energy integrated Green's functions,

$$\hat{g} = \frac{i}{\pi}\int d\xi \hat{\gamma}\cdot\hat{\mathcal{G}}, \tag{15}$$

where $\hat{\gamma}$ is a 4×4 diagonal matrix with elements $(1,-1,-1,1)$. In compact matrix form the quasiclassical equation reads,

$$\begin{aligned}&\left[\left(\omega + \frac{e}{ic}\mathbf{v}_F\cdot\mathbf{A}\right)\hat{\gamma},\hat{g}\right] + \mathbf{v}_F\cdot\nabla\hat{g} \\ &+ i\left[(\hat{\mathcal{H}}_\delta + \hat{\mathcal{H}}_{\rm sc} + \hat{\mathcal{H}}_{\rm sdw})\hat{\gamma},\hat{g}\right] = 0,\end{aligned} \tag{16}$$

where $\mathbf{v}_F$ is the Fermi velocity and $\mathbf{A}$ is the vector potential. $\hat{\mathcal{H}}_{\rm sc}$, $\hat{\mathcal{H}}_{\rm sdw}$ are the SC and the SDW components of the mean-field Hamiltonian in the basis spanned by Ψ. $\hat{\mathcal{H}}_\delta$ is a 4×4 diagonal matrix with elements (0,0,2δ,-2δ) containing information about nesting between the Fermi surfaces. Its contribution drops out in the absence of the SDW order. This equation agrees with one derived by Moor *et al.*[50]. In the pure superconducting limit Eq. (16) reduces to the well-known Eilenberger equation,

$$\mathbf{v}_F\cdot\nabla\hat{g} + \left[\left(\omega + \frac{e}{ic}\mathbf{v}_F\cdot\mathbf{A}\right)\hat{\gamma},\hat{g}\right] + i\left[\hat{\mathcal{H}}_{\rm sc}\hat{\gamma},\hat{g}\right] = 0. \tag{17}$$

Equation (16) has to be supplemented with the normalization condition,

$$\hat{g}^2 = \hat{g}^2_{bulk}. \tag{18}$$

In particular, $\hat{g}^2_{bulk} = \hat{\mathbb{1}}$ for a uniform superconductor without SDW order. The self-consistency conditions for the order parameters can be expressed in terms of the Eilenberger functions as,

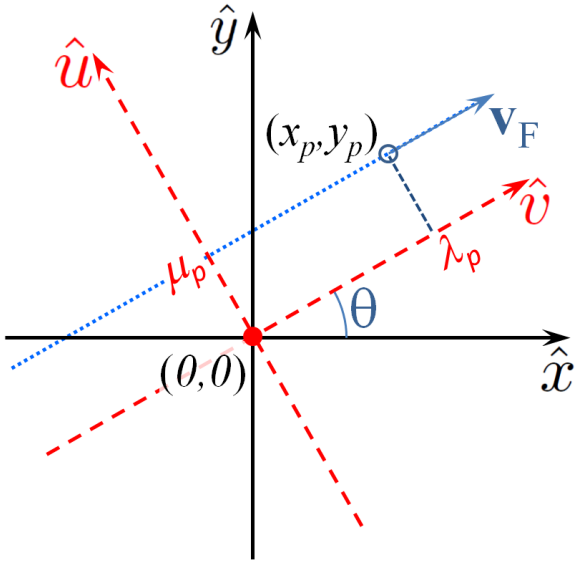

FIG. 2. (Color online) Coordinate systems used to solve the Eilenberger equations. The real space lab frame is shown with solid lines, while the dashed lines represent the new coordinate system. Filled circle is the location of the vortex core and chosen as the origin. Open circle is the point where the solution is required. A point in the lab frame $r = x_p\hat{x} + y_p\hat{y}$ maps to $\lambda_p\hat{v} + \mu_p\hat{u}$ in the new coordinate system.

$$\Delta_1 = i\pi T\sum_\omega \langle V^{\rm sc}_{11}g_{12} + V^{\rm sc}_{12}g_{34}\rangle_{F.S.}, \tag{19}$$

$$\Delta_2 = i\pi T\sum_\omega \langle V^{\rm sc}_{12}g_{12} + V^{\rm sc}_{22}g_{34}\rangle_{F.S.}, \tag{20}$$

$$M = i\pi T\sum_\omega \frac{V^{\rm sdw}}{2}\langle g_{13} + g_{24}\rangle_{F.S.}. \tag{21}$$

Here g_{ij} are components of 4×4 matrix Green's function (indices $i,j = (1,2)/(3,4)$ correspond to the hole/electron band). $\langle g_{ij}\rangle_{F.S.}$ means angular average over the Fermi surface for the respective bands weighted with the density of states, which is approximately the same for the both bands for the Fermi surfaces considered here. As for the pairing-interaction matrix, to get the $s_\pm$ superconducting state we take into account only the interband repulsive interaction and neglect intraband terms, i.e., $V^{\rm sc}_{11} = V^{\rm sc}_{22} = 0$. For pure SC state, Eq. (17) equations can be transformed to a set of Riccati equations, which makes the numerical solution much easier.[51] However this transformation is not useful for the problem considered here. In the following section, we discuss the strategy to solve these equations for the present case.

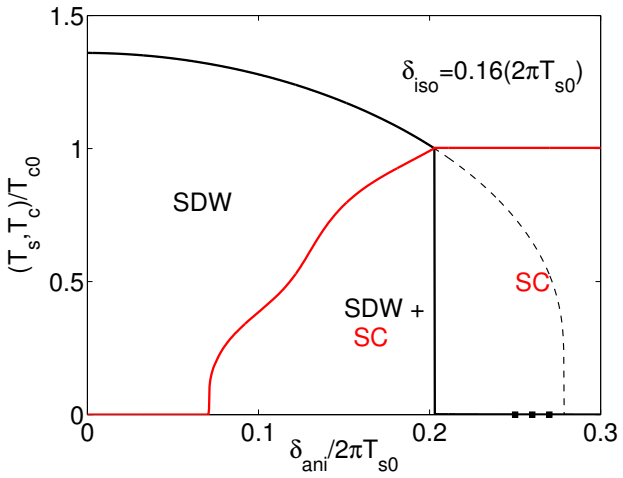

FIG. 3. (Color online) The phase diagram in the (T,$\delta_{\rm ani}$) plane for the two phases at zero magnetic field. Thick black/red line indicates transition to the SDW/SC state. The thin dashed line shows the T_s in the absence of the SC correlations. Filled squares are considered as representative cases in this paper.

B. Numerical solution

The Eilenberger equations are first-order partial differential equations. A standard tool for solution of this type of equations is the method of characteristics. The basic idea of this method is to introduce the new coordinate system, in which the partial differential equation reduces to an ordinary differential equation. Hence, it is useful to introduce a coordinate system spanned by the two orthogonal vectors, a unit vector along the direction of the Fermi velocity $\hat{v}$ and a unit vector $\hat{u}$ orthogonal to $\hat{v}$, see Fig. 2. The unit vectors spanning the new coordinate system read,

$$\hat{v} = \cos\theta\hat{x} + \sin\theta\hat{y}, \tag{22}$$
$$\hat{u} = -\sin\theta\hat{x} + \cos\theta\hat{y}. \tag{23}$$

Here θ is the angle between the Fermi velocity and the x axis in the lab frame. A point in the lab frame $\mathbf{r} = (x, y)$ maps to (λ, μ) in the $\hat{v}$-$\hat{u}$ frame. A point (x_p, y_p) at which solution is desired transforms to (λ_p, μ_p) as,

$$\lambda_p = x_p\cos\theta + y_p\sin\theta, \tag{24}$$
$$\mu_p = -x_p\sin\theta + y_p\cos\theta, \tag{25}$$

where the parameter μ_p has the meaning of an impact parameter. For a fixed trajectory, this impact parameter is uniquely determined by (x_p, y_p) and it does not change with change of λ. The quasiclassical equations are solved along these classical trajectories $(\hat{v})$ in the real space. Along such trajectories quasiclassical equations reduce to system of ordinary differential equations, which are much easier to handle than solving a set of partial differential equations. Far away from the bulk, the system is homogeneous. The homogeneous values are used as initial values. Now on a given trajectory, there are two possibilities. One can integrate towards the defect (vortex in this case) from the two extreme ends ($\lambda = \pm\infty$) of the trajectory. Due to the first-order nature of the equations, the numerical solution readily converges to exponentially growing function. Of course, these exponentially growing solutions are unphysical. However, it is possible to construct the physically bounded solution at any point using the exponentially growing solution using the explosion method. The explosion method exploits exponentially growing solutions to obtain the physical solution.[52–54] (See Appendix A for details) For each point in the real space, one has to solve the Eilenberger equations for all the trajectories and for each Matsubara frequency. To obtain a physical solution, we solve the Eilenberger equations from two opposite directions $\lambda = \pm\infty$ towards the point, where the solution is desired. As shown in the Appendix, the two exploding solutions $\hat{g}_\pm$ diverging in the $\pm\infty$ limits, provide the physical solution $\hat{g}_p$ as

$$\hat{g}_p = \frac{\hat{g}_-\hat{g}_+ - \hat{g}_+\hat{g}_-}{\hat{g}_-\hat{g}_+ + \hat{g}_+\hat{g}_-}. \tag{26}$$

Once all the Eilenberger functions are computed for an initial guess for the order parameters, an updated set of order parameters is recalculated, and this process continues till it converges to a solution. It is convenient to normalize all the energy scales to T_c and all the lengths are measured in the unit of superconducting coherence length $\xi_0 = v_F/(2\pi T_c)$. Here v_F is the average Fermi velocity of the two bands. We consider weak ellipticity for the electronlike Fermi surface, and the Fermi velocities of the two bands are roughly equal. All our results are presented in these units.

III. RESULTS & DISCUSSION

Coexistence of the SDW state and the superconductivity is very sensitive to the underlying electronic structure. For the two-band model we consider, the nesting function $\delta(\phi)$ in Eq. (5) can be tuned to get a co-existing phase.[45–47] Here we are interested in a situation where there is no long-range SDW order in the absence of the magnetic field. Fig. 3 shows the phase diagram as a function of the anisotropic nesting parameter $\delta_{\rm ani}$ for a fixed value of $\delta_{\rm iso} = 0.16(2\pi T_{s0})$. The presence of the superconductivity strongly modifies the SDW phase boundary (thin dashed line in Fig. 3). The region between the original and SC-renormalized phase boundaries provides a possibility of the SDW order in the regions, where the SC phase get suppressed locally. The phase diagram shown in Fig. 3 is only includes the commensurate SDW phase. Vorontsov *et al.*[46] have shown that the incommensurate SDW phase may co-exist with the SC in a larger area of the phase diagram. We consider few representative cases with $\delta_{\rm ani}/2\pi T_{s0} = 0.25, 0.26$ and 0.27. Here T_{s0} is the SDW transition temperature for a system with perfect nesting and with the same interaction

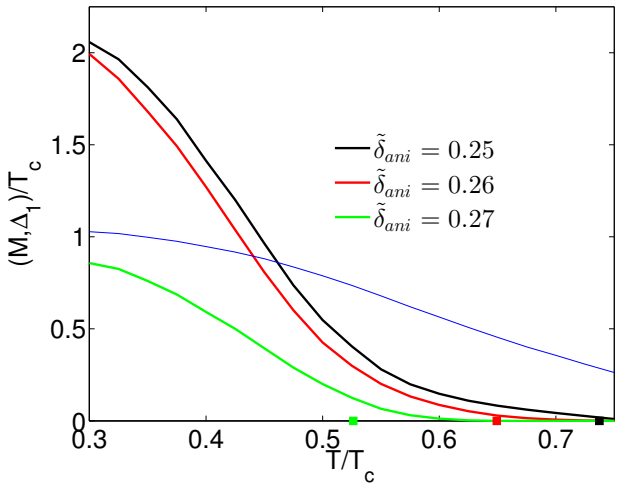

FIG. 4. (Color online) The temperature dependence of the bulk superconducting order parameter and the SDW orders at the center of the vortex for three values of the parameter $\delta_{\rm ani}/2\pi T_{s0}$= 0.25,0.26 and 0.27. All the energy scales are normalized to T_c. The thin line shows the temperature dependence of the magnitude of the SC order in the bulk, which is almost identical for two bands. This signs of SC order parameters are opposite for two bands. The mean-field SDW transition temperature in the absence of superconductivity is indicated with filled square for each case.

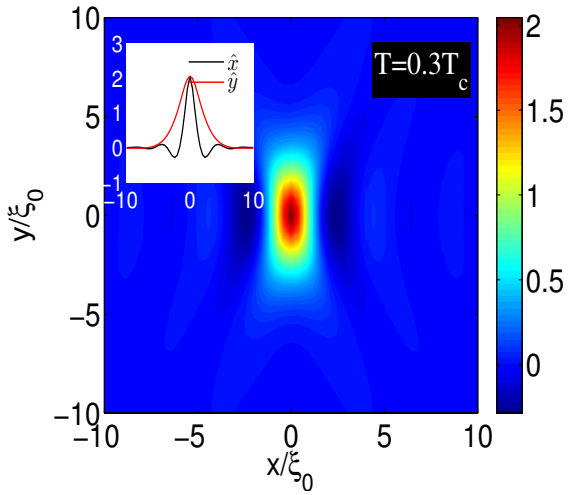

FIG. 5. (Color online) The spatial variation of the magnitude of the SDW order at $T = 0.3T_c$ for $\delta_{\rm ani} = 0.25(2\pi T_{s0})$, where T_{s0} is the SDW transition temperature for a system with perfect nesting and with the same interaction strength. The magnitude of the SDW order is normalized to T_c. The hot spots are located near the y-axis.

strength. We have set $T_{s0} = 2T_{c0}$, where T_{c0} is the superconducting temperature. As we are mostly interested in low-temperature behavior, we restrict our calculations below $T = 0.8T_c$.

A. Order parameter profiles

Fig. 4 shows the temperature dependence of the bulk superconducting gap and the SDW order in the core. It is evident that the SDW order appears roughly below the temperature one would expect from the phase diagram shown in Fig. 3. The temperature dependence of the SDW order parameter deviates strongly from the mean-field behavior ($\propto \sqrt{1-T/T_c}$). We see two different temperature regimes. At lower temperature the SDW order grows strongly, but slightly below the mean-field SDW transition T_s it develops a tail, which survives even above T_s. It should be noted here that the phase diagram is based on the commensurate SDW phase for the normal state electronic structure. However, the electronic structure of the vortex core states is not the same as in the normal state. The onset of the SDW order is mostly determined by the core bound states. The SDW transition temperature $T_s \propto \exp[-1/N_0 V_{\rm sdw} f(\delta_{\rm iso}, \delta_{\rm ani})]$, where the function $f(\delta_{\rm iso}, \delta_{\rm ani})$ depends on nesting parameters, $V_{\rm sdw}$ is the SDW interaction and N_0 is the density of states. As in the vortex core the density of states is higher than the normal-state value, the SDW onset temperature may exceed the mean-field value.

We restrict ourselves to the commensurate case only, but for the incommensurate case the phase boundary shifts towards slightly higher temperatures. As reported by Vorontsov *et al.* in Ref. 46, an incommensurate order may exist in a larger portion of the phase diagram. We have also performed calculations, where we allow incommensurability in the SDW order. With incommensurability the SDW order parameter becomes complex and acquires a finite phase. We found that the phase of the SDW order parameter is temperature dependent and varies very weakly in the real space. The incommensurate order persists above the phase boundary shown in Fig. 3. Since we did not find anything qualitatively different, we will focus on the commensurate case only. Furthermore, there is no qualitative difference between the cases considered here, except for the temperature dependence. Therefore, we continue our discussion with $\delta_{\rm ani}/2\pi T_{s0} = 0.25$. For this $\delta_{\rm ani}$ and $\delta_{\rm iso}/2\pi T_{s0} = 0.16$ the nesting hot-spot angle $\phi \approx 64.9°$ is close to the y direction which strongly influences anisotropic properties of the vortex. Figure 5 shows the magnetic field-induced SDW order parameter in the real space at $T = 0.3T_c$. Spatial coordinates have been normalized to the superconducting coherence length ξ_0 and the SDW order is normalized to T_c. An important feature is the oscillations of the SDW order along the x direction which is most clearly seen in the inset. At lower temperatures when the SC vortex is very small, the SDW state is localized very close to the vortex core. As the temperature grows, vortex becomes larger and the region with the SDW order also increases, due to a larger region of the suppressed superconductivity. The size of the vortex is larger in the presence of the field-induced SDW order. This property can be seen in Fig. 6, in which we compare

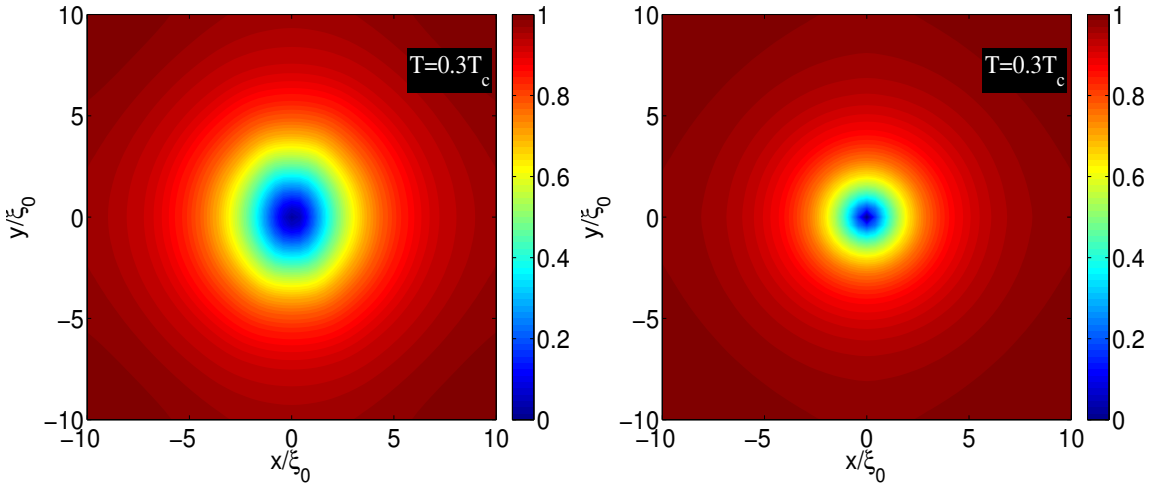

FIG. 6. (Color online) The left panel shows the gap magnitude normalized to its bulk value at $T = 0.3T_c$ in the presence of the SDW order and the right panel shows the gap structure at the same temperature with no SDW order for the hole band.

a SC vortex with and without the magnetic field-induced SDW order. The SDW order makes vortex larger and anisotropic. The intrinsic anisotropy of the underlying band structure is weak. Hence the large anisotropy in the real space is mainly due to the field-induced SDW order. Strong enhancement of the anisotropy is reflected in the characteristic length scales associated with the SC order along the two principal directions. Fig. 7 shows the length scales associated with the SDW ($\xi^{\rm sdw}_{x/y}$) and the SC order ($\xi^{\rm sc}_{x/y}$) along the x and y axis. We define the superconducting coherence length $\xi_{\rm sc}$ as a distance from the vortex core, where the order parameters reaches half of its bulk value. Similarly, the magnitude of the SDW order drops to half of its value at the core at a distance $\xi_{\rm sdw}$ from the vortex core. As illustrated in Fig. 7, the SC length scales along x and y directions become different in the presence of the SDW order and this is mainly due to anisotropy in the field-induced SDW order. Note that the SDW correlations are stronger along the y direction which is closer to the nesting hot spots. This causes stronger suppression of the SC order and reduces the SC characteristic length along this direction. Next, we discuss the density of states near the vortex core.

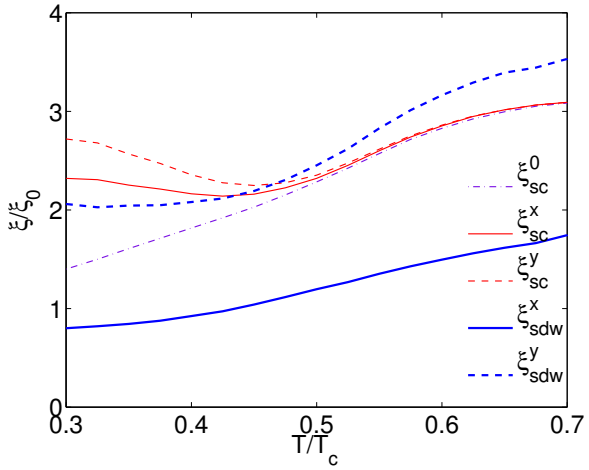

FIG. 7. (Color online) The temperature dependence of characteristic length scale for SDW order ($\xi^{\rm sdw}_{x/y}$) and the characteristic length scale of the SC order ($\xi^{\rm sc}_{x/y}$) on the hole band for $\delta_{\rm ani}/2\pi T_{s0} = 0.25$. Subscripts denotes x and y directions in the real space. The same characteristic length scale for a pure superconductor is plotted with a dotted dashed line for comparison.

B. Density of states

All the previous calculations were done using the Matsubara frequencies. For the DOS calculation it is necessary to go to the real frequencies. We used the order parameter profiles calculated in the Matsubara representation. The analytic continuation, $i\omega \to E + i\eta$, is done with an artificial broadening $\eta = 0.05T_c$. This process also requires solution of the Eilenberger equations for the real frequencies using the same approach as in the calculation of the order parameters in the previous section. The total DOS is the sum of the partial DOSs for each band and, in terms of the Eilenberger functions, it is given by

$$N(E) = {\rm Re}\langle [g_{11}(E + i\eta) + g_{33}(E + i\eta)]\rangle_{FS}. \qquad (27)$$

Fig. 8 presents evolutions of the density of states along the two principal directions for two temperatures. The first row of Fig. 8 shows DOS along the x axis, which is away from the hot spots and the second row shows DOS along the y axis which is closer to the hot spots. The field-induced SDW order enhances the violation of the C_4 rotational symmetry the vortex center. For conventional superconductors, the DOS is always particle-hole

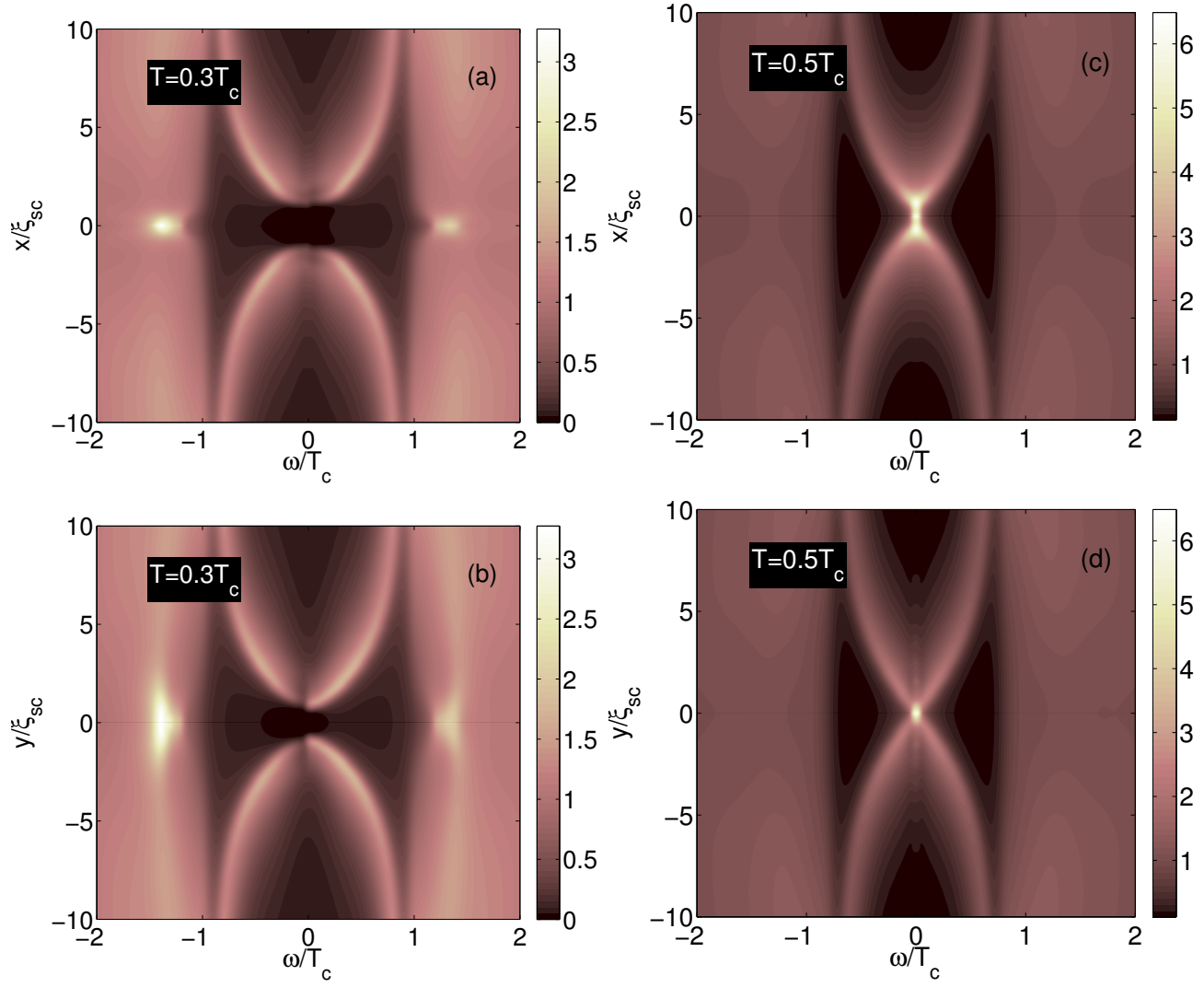

FIG. 8. (Color online) DOS along the x direction (first row) and along y direction (second row) at T=0.3T_c in panel (a), (b) and at T=0.5T_c in panel (c) and (d) for $\delta_{ani}/2\pi T_c$=0.26.

symmetric, unless the superconductor is in the quantum regime when $k_F\xi_0$ is not too large and $T \ll T_c/k_F\xi_0$.[39] Another key feature of the classical clean-limit DOS in the vortex core is the sharp peak at zero energy corresponding to the localized state. The quantum effects shift this zero-bias peak to the finite energy but, do not break the rotational symmetry. The emergence of the SDW order leads to particle-hole asymmetry in the DOS and also strongly violates the C_4 symmetry. The particle-hole asymmetry is bigger along x direction because of stronger deviation from nesting in this direction. Another important feature which is visible in the Fig. 8 is suppressed spectral weight at the core indicating that the energy of localized state is shifted from zero to a finite value corresponding to opening of a minigap in the core. This is shown more clearly in Fig. 9 in which we show the DOS plots at several representative points. This small gap in the DOS near the vortex core is particle-hole asymmetric, which is a hallmark of energy gap due to the SDW order. This gap vanishes away from the vortex core indicating presence of a state with energy close to zero localized outside the core. As the temperature increases and the SDW order weakens, the apparent gap in the core disappears as shown in panel (c) and (d) of Fig. 8 at T = 0.5T_c. The described features are the keys to distinguish between the quantum effect and the field-induced SDW order. Figure 8 also shows the DOS for two different temperatures. The temperature dependence of the DOS is easy to understand. As the temperature increases, the SDW order weakens, which reduces the degree of C_4 symmetry breaking and the particle-hole asymmetry in the DOS.

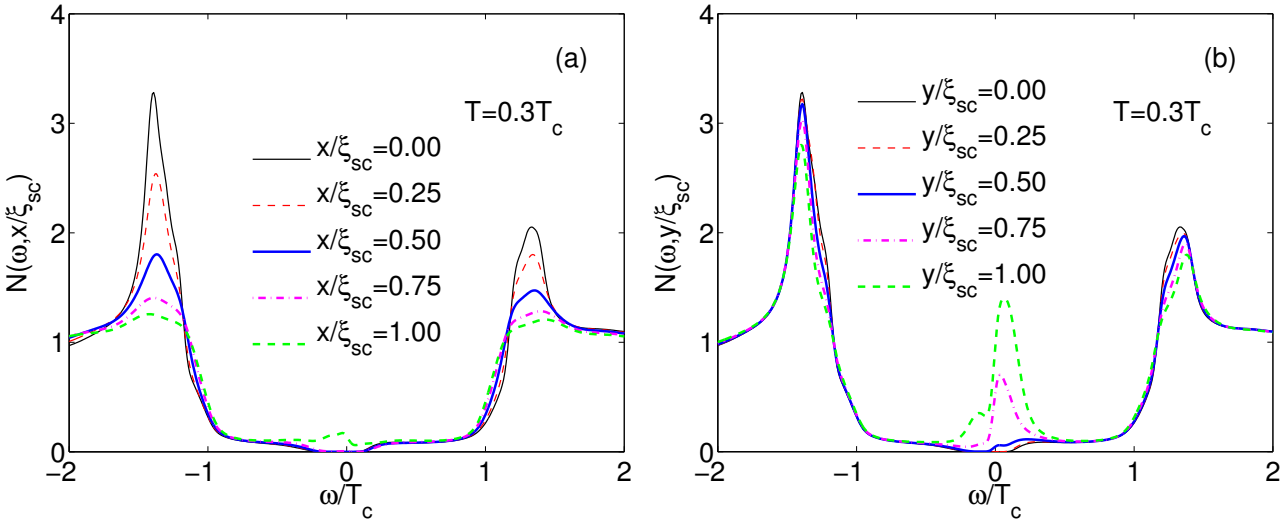

FIG. 9. (Color online) Panels (a) and (b) show DOS near the vortex core along x and y directions respectively at T=0.3T_c.

IV. SUMMARY AND CONCLUSION

We study the structure of an isolated superconducting vortex near a SDW instability inside the superconducting dome. We show that the SDW order develops inside the vortex below a critical temperature determined by the strength of the SDW instability. This leads to C_4 symmetry breaking near the vortex core. If there is already C_4 breaking in underlying band structure, then it gets strongly enhanced due to the SDW order near the vortex core. The corresponding deformation of the vortex shape can be imaged by the STM technique. We find that the field-induced SDW order persists beyond the superconducting vortex region. The tunneling DOS carries very strong signatures of this field-induced order. A small energy gap develops inside the core and gives rise to strong particle hole asymmetry, which is pronounced along the directions away from the hot spots. Our results are in qualitative agreement with the STM data on on $Ba_{0.6}K_{0.4}Fe_2As_2$[34] which may indicate the presence of the vortex-core SDW order in this material. Our findings also agree with BdG-based works by other groups.

ACKNOWLEDGMENTS

This work was supported by the Center for Emergent Superconductivity, an Energy Frontier Research Center funded by the US DOE, Office of Science, under Award No. DE-AC0298CH1088.

Appendix A: Explosion method

The general structure of the Eilenberger equations is,

$$\frac{d\hat{g}}{d\lambda} = [\mathcal{T}, \hat{g}]\,, \tag{A1}$$

which is a first-order ordinary differential equation. It is straightforward to show that if $\hat{g}$ is a solution of this equation then $\hat{g}^2$ is also a solution, which implies

$$\hat{g}^2 = \hat{a}_0 + a_1\hat{g}, \tag{A2}$$

where $\hat{a}_0$ is a constant matrix and a_1 is a complex number. It can be further shown that the product of any two solutions of the Eilenberger equations is also a solution of these equations. This gives a very powerful relation,

$$\hat{g}^2 = \hat{a}_0 = \hat{g}^2_{bulk}, \tag{A3}$$

which is very useful in obtaining the numerical solutions of these equations. There are multiple solutions to this system of equations. In pure superconducting state, there are three independent solutions. There are two divergent solutions along with a bounded physical solution. All the unphysical solutions decay to zero in the bulk. Let's consider two such unphysical solutions, $\hat{g}_\pm \propto e^{\pm\nu\lambda}$. It can be shown that commutator of these two unphysical solutions gives the physically bounded solution,

$$\hat{X}_\pm = \hat{g}_-\hat{g}_+ \pm \hat{g}_+\hat{g}_-, \tag{A4}$$

$$\hat{\dot{X}}_\pm = [\mathcal{T}, \hat{X}_\pm]. \tag{A5}$$

The bounded physical solution is,

$$\hat{g}_p = \hat{c}_p\hat{X}_-, \tag{A6}$$

the constant $\hat{c}_p$ can be determined using Eq. (A3) and (A6) and it reads,

$$\hat{c}_p = \frac{1}{\hat{X}_+}. \tag{A7}$$

We use these unphysical solutions $\hat{g}_{+,-}$ in the bulk and integrate towards the vortex core starting from the bulk. Since these solutions grow exponentially, they can be easily computed numerically with appropriate boundary conditions. Far away from defects, we can ignore the spatial dependence of the order parameters. Since there is no long-range SDW order, we have the standard Eilenberger equations for the pure superconducting state in the bulk and in the basis we consider here, the Eilenberger Green's function is a block diagonal matrix. The two bands are coupled through the self-consistency condition. Therefore it is sufficient to illustrate the idea for one band, for which we write down the equations explicitly,

$$\dot{g} = i\left(\Delta^* f + \Delta f^\dagger\right), \tag{A8}$$
$$\dot{f} = -2\omega f - 2i\Delta g, \tag{A9}$$
$$\dot{f}^\dagger = 2\omega f^\dagger - 2i\Delta^* g. \tag{A10}$$

We first find two unphysical solutions, which can be determined easily. Let's consider,

$$g = c_1 e^{\zeta\lambda}, \tag{A11}$$
$$f = c_2 e^{\zeta\lambda}, \tag{A12}$$
$$f^\dagger = c_3 e^{\zeta\lambda}. \tag{A13}$$

where $\zeta = \pm\nu$. Normalization condition requires,

$$\hat{g}_\pm^2 = 0. \tag{A14}$$

This ensures that all the unphysical solution decay to zero in the bulk. Which gives,

$$c_1^2 + c_2 c_3 = 0, \tag{A15}$$
$$c_1 = i\sqrt{c_2 c_3}. \tag{A16}$$

Using these conditions,

$$(\zeta + 2\omega)c_2 = 2\Delta\sqrt{c_2 c_3}, \tag{A17}$$
$$(\zeta - 2\omega)c_3 = 2\Delta^*\sqrt{c_2 c_3}. \tag{A18}$$

These two equations give the value of $\zeta = \pm 2\sqrt{\omega^2 + |\Delta|^2}/v_F$ and

$$c_2 = \tfrac{-2i\Delta}{\zeta v_F + 2\omega} c_1, \tag{A19}$$
$$c_3 = \tfrac{-2i\Delta^*}{\zeta v_F - 2\omega} c_1. \tag{A20}$$

Here we fix $c_1 = 1$ and write the exploding solutions,

$$\hat{g}_+ = \exp\left[+\frac{2Q\lambda}{v_F}\right]\begin{bmatrix} 1 & -i\Delta p_+ \\ i\Delta^* p_- & -1 \end{bmatrix}, \tag{A21}$$

$$\hat{g}_- = \exp\left[-\frac{2Q\lambda}{v_F}\right]\begin{bmatrix} 1 & -i\Delta p_- \\ i\Delta^* p_+ & -1 \end{bmatrix}, \tag{A22}$$

$$p_\pm = \frac{1}{\omega \pm Q}, \tag{A23}$$
$$Q = \sqrt{\omega^2 + |\Delta|^2}. \tag{A24}$$

Now we can write down the physical solution,

$$\hat{g}_p = \frac{\hat{X}_-}{\hat{X}_+} = \frac{1}{\sqrt{\omega^2 + |\Delta|^2}}\begin{bmatrix} \omega & -i\Delta \\ i\Delta^* & -\omega \end{bmatrix} \tag{A25}$$

Once we get the values of these two diverging solutions in bulk then we can use the bulk values to integrate towards the vortex core and find the physical solution using two unphysical solutions.

[1] D. C. Johnston, Advances in Physics **59**, 803 (2010).
[2] P. C. Canfield and S. L. Bud'ko, Annual Review of Condensed Matter Physics **1**, 27 (2010).
[3] P. J. Hirschfeld, M. M. Korshunov, and I. I. Mazin, Reports on Progress in Physics **74**, 124508 (2011).
[4] G. R. Stewart, Rev. Mod. Phys. **83**, 1589 (2011).
[5] H.-H. Wen and S. Li, Annual Review of Condensed Matter Physics **2**, 121 (2011).
[6] A. Chubukov, Ann. Rev. Cond. Mat. Phys. **3**, 57 (2012).
[7] Ø. Fischer, M. Kugler, I. Maggio-Aprile, C. Berthod, and C. Renner, Rev. Mod. Phys. **79**, 353 (2007).
[8] J. E. Hoffman, E. W. Hudson, K. M. Lang, V. Madhavan, H. Eisaki, S. Uchida, and J. C. Davis, Science **295**, 466 (2002).
[9] B. Lake, G. Aeppli, K. N. Clausen, D. F. McMorrow, K. Lefmann, N. E. Hussey, N. Mangkorntong, M. Nohara, H. Takagi, T. E. Mason, and A. Schröder, Science **291**, 1759 (2001).
[10] B. Khaykovich, Y. S. Lee, R. W. Erwin, S.-H. Lee, S. Wakimoto, K. J. Thomas, M. A. Kastner, and R. J. Birgeneau, Phys. Rev. B **66**, 014528 (2002).
[11] B. Lake, H. M. Rønnow, N. B. Christensen, G. Aeppli, K. Lefmann, D. F. McMorrow, P. Vorderwisch, P. Smeibidl, N. Mangkorntong, T. Sasagawa, M. Nohara, H. Takagi, and T. E. Mason, Nature (London) **415**, 299 (2002).
[12] J. M. Tranquada, C. H. Lee, K. Yamada, Y. S. Lee, L. P. Regnault, and H. M. Rønnow, Phys. Rev. B **69**, 174507 (2004).
[13] B. Khaykovich, S. Wakimoto, R. J. Birgeneau, M. A. Kastner, Y. S. Lee, P. Smeibidl, P. Vorderwisch, and K. Yamada, Phys. Rev. B **71**, 220508 (2005).
[14] J. Chang, A. P. Schnyder, R. Gilardi, H. M. Rønnow, S. Pailhes, N. B. Christensen, C. Niedermayer, D. F. McMorrow, A. Hiess, A. Stunault, M. Enderle, B. Lake, O. Sobolev, N. Momono, M. Oda, M. Ido, C. Mudry, and J. Mesot, Phys. Rev. Lett. **98**, 077004 (2007).
[15] J. Chang, C. Niedermayer, R. Gilardi, N. B. Christensen, H. M. Rønnow, D. F. McMorrow, M. Ay, J. Stahn, O. Sobolev, A. Hiess, S. Pailhes, C. Baines, N. Momono, M. Oda, M. Ido, and J. Mesot, Phys. Rev. B **78**, 104525 (2008).

[16] V. F. Mitrovic, E. E. Sigmund, W. P. Halperin, A. P. Reyes, P. Kuhns, and W. G. Moulton, Phys. Rev. B **67**, 220503 (2003).
[17] D. Haug, V. Hinkov, A. Suchaneck, D. S. Inosov, N. B. Christensen, C. Niedermayer, P. Bourges, Y. Sidis, J. T. Park, A. Ivanov, C. T. Lin, J. Mesot, and B. Keimer, Phys. Rev. Lett. **103**, 017001 (2009).
[18] T. Wu, H. Mayaffre, S. Krämer, M. Horvatić, C. Berthier, W. N. Hardy, R. Liang, D. A. Bonn, and M.-H. Julien, Nature (London) **477**, 191 (2011).
[19] J. Chang, E. Blackburn, A. T. Holmes, N. B. Christensen, J. Larsen, J. Mesot, R. Liang, D. A. Bonn, W. N. Hardy, A. Watenphul, M. V. Zimmermann, E. M. Forgan, and S. M. Hayden, Nature Physics **8**, 871 (2012).
[20] D. Leboeuf, S. Krämer, W. N. Hardy, R. Liang, D. A. Bonn, and C. Proust, Nature Physics **9**, 79 (2012).
[21] T. Wu, H. Mayaffre, S. Krämer, M. Horvatić, C. Berthier, P. L. Kuhns, A. P. Reyes, R. Liang, W. N. Hardy, D. A. Bonn, and M.-H. Julien, Nature Communications **4**, 2113 (2013).
[22] K. Kakuyanagi, K.-i. Kumagai, and Y. Matsuda, Phys. Rev. B **65**, 060503 (2002).
[23] K. Kakuyanagi, K. Kumagai, Y. Matsuda, and M. Hasegawa, Phys. Rev. Lett. **90**, 197003 (2003).
[24] D. P. Arovas, A. J. Berlinsky, C. Kallin, and S.-C. Zhang, Phys. Rev. Lett. **79**, 2871 (1997).
[25] S. Sachdev and E. Demler, Phys. Rev. B **69**, 144504 (2004).
[26] A. Ghosal, C. Kallin, and A. J. Berlinsky, Phys. Rev. B **66**, 214502 (2002).
[27] J.-X. Zhu and C. S. Ting, Physical Review Letters **87**, 147002 (2001).
[28] H.-Y. Chen and C. S. Ting, Phys. Rev. B **71**, 220510 (2005).
[29] W. A. Atkinson and J. E. Sonier, Phys. Rev. B **77**, 024514 (2008).
[30] M. Schmid, B. Andersen, A. Kampf, and P. Hirschfeld, New Journal of Physics **12**, 053043 (2010).
[31] V. V. Garkusha and V. N. Krivoruchko, Journal of Low Temperature Physics **139**, 37 (2005).
[32] J. E. Hoffman, Rep. Prog. Phys. **74**, 124513 (2011).
[33] Y. Yin, M. Zech, T. L. Williams, X. F. Wang, G. Wu, X. H. Chen, and J. E. Hoffman, Phys. Rev. Lett. **102**, 097002 (2009).
[34] L. Shan, Y.-L. Wang, B. Shen, B. Zeng, Y. Huang, A. Li, D. Wang, H. Yang, C. Ren, Q.-H. Wang, S. Pan, and H.-H. Wen, Nat. Phys. **7**, 325 (2011).
[35] T. Hanaguri, K. Kitagawa, K. Matsubayashi, Y. Mazaki, Y. Uwatoko, and H. Takagi, Phys. Rev. B **85**, 214505 (2012).
[36] C.-L. Song, Y.-L. Wang, P. Cheng, Y.-P. Jiang, W. Li, T. Zhang, Z. Li, K. He, L. Wang, J.-F. Jia, H.-H. Hung, C. Wu, X. Ma, X. Chen, and Q.-K. Xue, Science **332**, 1410 (2011).
[37] M. A. N. Araújo, M. Cardoso, and P. D. Sacramento, New J. Phys. **11**, 113008 (2009).
[38] D. Wang, J. Xu, Y.-Y. Xiang, and Q.-H. Wang, Phys. Rev. B **82**, 184519 (2010).
[39] N. Hayashi, T. Isoshima, M. Ichioka, and K. Machida, Phys. Rev. Lett. **80**, 2921 (1998).
[40] H.-H. Hung, C.-L. Song, X. Chen, X. Ma, Q.-k. Xue, and C. Wu, Phys. Rev. B **85**, 104510 (2012).
[41] D. Chowdhury, E. Berg, and S. Sachdev, Phys. Rev. B **84**, 205113 (2011).
[42] H.-M. Jiang, J.-X. Li, and Z. D. Wang, Phys. Rev. B **80**, 134505 (2009).
[43] X. Hu, C. S. Ting, and J.-X. Zhu, Phys. Rev. B **80**, 014523 (2009).
[44] Y. Gao, H.-X. Huang, C. Chen, C. S. Ting, and W.-P. Su, Phys. Rev. Lett. **106**, 027004 (2011).
[45] A. B. Vorontsov, M. G. Vavilov, and A. V. Chubukov, Phys. Rev. B **79**, 060508 (2009).
[46] A. B. Vorontsov, M. G. Vavilov, and A. V. Chubukov, Phys. Rev. B **81**, 174538 (2010).
[47] R. M. Fernandes and J. Schmalian, Phys. Rev. B **82**, 014521 (2010).
[48] G. Eilenberger, Z. Phys. **214**, 195 (1968).
[49] A. I. Larkin and Y. N. Ovchinnikov, Sov. Phys. JETP **28**, 1200 (1969).
[50] A. Moor, A. F. Volkov, and K. B. Efetov, Phys. Rev. B **83**, 134524 (2011).
[51] N. Schopohl, arXiv:cond-mat/9804064 , (1998).
[52] E. V. Thuneberg, J. Kurkijärvi, and D. Rainer, Phys. Rev. B **29**, 3913 (1984).
[53] W. Zhang, J. Kurkijärvi, and E. V. Thuneberg, Phys. Rev. B **36**, 1987 (1987).
[54] U. Klein, J. of Low Temp. Phys. **69**, 1 (1987).